Student symposium

Thursday, November 26

Session I

SL1

Phase diagram and temperature evolution of structure and modulation of $Ni_2MnGa_{1-x}In_x$ single crystals

FÁZOVÝ DIAGRAM TEPLOTA VS. KOMPOZICE A TEPLOTNÍ VÝVOJ STRUKTURY A MODULACE NA MONOKRYSTALECH $Ni_2MnGa_{1-x}In_x$

Petr Cejpek, Petr Doležal, Petr Opletal, Jaroslav Valenta, Kristina Vlášková, Milan Dopita

Faculty of Mathematics and Physics, Charles University, Ke Karlovu 5, 121 16 Praha 2

Slitiny s tvarovou pamětí založené na sloučeninách Ni-Mn-Ga jsou v posledních letech intenzivně studovány díky jejich potenciálnímu využití jako aktuátory, senzory nebo například mikropumpy [1-2]. Vlastnosti těchto materiálů jsou spojeny s martensitickou transformací, při které dochází k transformaci z kubické austenitické fáze do martensitu, který má nižší symetrii [3]. Ve většině případů martensit vykazuje rovněž modulaci ve struktuře [4]. Pomocí různých dopování byla objevena výrazná závislost vlastností a kritických teplot na kompozici, nicméně většina těchto studií byla provedena na polykrystalických vzorcích.

Monokrystaly $Ni_2MnGa_{1-x}In_x$ pro tuto studii byly připraveny pomocí Bridgmanovy metody. Teploty transformací byly zjiš ovány pomocí měření magnetizace a elektrického odporu. Curieho teplota a teploty pre-martensitické a martensitické transformace klesají se vzrůstajícím obsahem india ve vzorcích. Tento pokles je mnohem rychlejší než pokles publikovaný dříve na polykrystalických vzorcích, jelikož u našich monokrystalů nebyla pozorovana martensitická transformace na žádném vzorku s obsahem india větším než $x > 0.05$. Výsledky rentgenové difrakce měřené v nízkoteplotní martensitické fázi ukazují na jasný pokles monoklinního mřížového parametru a a nárůst parametrů c a v závislosti na zvyšujícím se obsahu india. Závislost na kompozici byla pozorována rovněž u modulačního vektoru v martensitické i pre-martensitické fázi, kde jeho x-ová a y-ová souřadnice nabývají hodnot 3/7 (martensit) a 1/3 (pre-martensit).

1. A. R. Smith, et al., Microfluidic. Nanofluidics 18 (2005) 1255, https://doi.org/10.1007/s10404-014-1524-6.
2. A. Hobza, et al., Sensor. Actuator. A 269 (2018) 137, https://doi.org/10.1016/j.sna.2017.11.002.
3. G. B. Olson, W. S. Owen, Martensite, ASM International, Materials Park, OH, 1992.
4. O. Heczko, et al., Acta Mater. 115 (2016) 250-258, https://doi.org/10.1016/j.actamat.2016.05.047.

SL2

$CePt_2Al_2$ - STRUCTURAL PROPERTIES

Petr Doležal, Elen Duverger-Nedellec, Stanislav Daniš, Pavel Javorský

Faculty of Mathematics and Physics, Charles University, Ke Karlovu 5, 121 16 Prague 2

This work is focused on the structural and physical properties of $CePt_2Al_2$, an intermetallic compound. $CePt_2Al_2$ belongs to the Ce based 1:2:2 compounds, which crystalize in the structural model of $CaBe_2Ge_2$ type, see Fig.1 At low temperature this structure type becomes very often unstable and result in the structural phase transition from tetragonal to an orthorhombic structure as for example in $CePd_2Al_{2-x}Ga_x$ series.

$CePt_2Al_2$ is a new member of this family and behaves in different way. At room temperature the structure is orthorhombic and modulated as was determined by single-crystal X-ray diffraction (*Cmme*(a00)000, with $\vec{q}$ = (0.481, 0, 0)). The dependence of lattice parameters above room temperature was studied by X-ray powder diffraction showing the presence of structural transition to a tetragonal structure above room temperature, which could be presumably describe by $CaBe_2Ge_2$ structure type. This transition exhibits 50 °C hysteresis and creates a domain structure in the sample. During the transition both tetragonal and orthorhombic phases coexist and their ratio is dependent on cooling rate.

The investigation was also focused on specific heat, magnetization, and transport measurements in the temperature range between 0.5 and 300 K. Specific heat and magnetic susceptibility show an antiferromagnetic order below 2 K. Around 20 K the temperature dependence of electrical

resistivity exhibits an upturn in typical metallic behaviour, which leads to the creation of local minimum. On the basis of electrical resistivity and other bulk measurements, $CePt_2Al_2$ can be considered a Kondo lattice material, for which the reduction of free magnetic Ce^{3+} moment is typical. The presence of a modulated crystal structure opens the possibility of a charge density wave state in $CePt_2Al_2$ as observed for (Re)Pt_2Si_2.

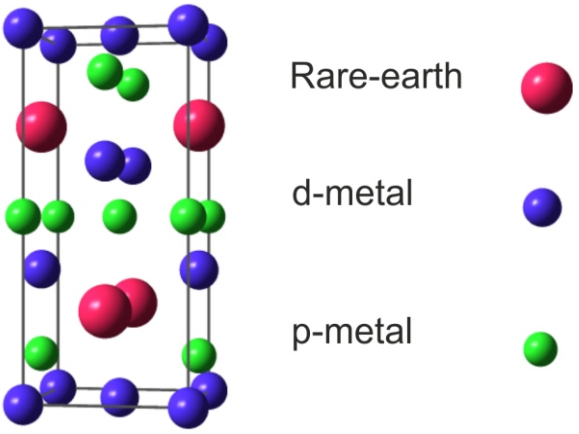

Figure 1. One of the most frequent structural model in RT_2X_2 (*R*: rare-earth, *T*: d-metal, *X*: p-metal) family of intermetallic compounds.

SL3

THE ALL-NEW FITEXC: MS EXCEL-BASED DIFFRACTION PROFILE FITTING PROGRAM (COVID LOCKDOWN EDITION)

Petr Veřtát[1,2], Jan Drahokoupil[1,3], Oleg Heczko[2]

[1]*Department of Solid State Engineering, Faculty of Nuclear Sciences and Physical Engineering, Czech Technical University in Prague*

[2]*Department of Magnetic Measurements and Materials, Institute of Physics, Czech Academy of Sciences*

[3]*Department of Material Analysis, Institute of Physics, Czech Academy of Sciences*

vertapet@fjfi.cvut.cz

Analysis of single or multiple diffraction profiles represents a crucial part in diffraction data processing for experimental materials science. The topic looks simple at first sight, but it soon becomes complex when seeking the highest precision or dealing with complicated data. Two years ago, we have introduced *FitExc* – diffraction profile fitting program written in MS Excel. This lightweight yet complex tool, running immediately on any computer equipped with MS Office, was proved to be able to deal with the precise customizable fitting of 1D diffraction scans .

Now, we introduce a new version of the program with upgraded functionality. We have increased the maximum amount of profiles to be fitted at once, added new options for fitting strategy customization (e.g., weighted least squares method), and introduced many tweaks making the control of the program faster and more effective.

Altogether, we present an effective newly upgraded tool for the analysis of single or multiple diffraction profiles measured using a conventional powder diffractometer. Among others, applications of *FitExc* include the precise evaluation of lattice parameters of single crystals, dealing with overlapped reflections in multiphase samples or twinned crystals, processing of data for residual stress analysis, thermal expansion analysis or even fitting of *q*-scans [3]. The presented program is free to use and available upon request - please contact the corresponding author if interested.

This work was supported by the Grant Agency of the Czech Technical University in Prague [grant No. SGS19/190/OHK4/3T/14].

SL4

Study of real structure of laser-welded tool steel

STUDIUM REÁLNÉ STRUKTURY LASEREM NAVAŘENÉ NÁSTROJOVÉ OCELE

K. Trojan[1], J. Čapek[1], J. Čech[2], V. Ocelík[3], N. Ganev[1]

[1]*Katedra inženýrství pevných látek, Fakulta jaderná a fyzikálně inženýrská, České vysoké učení technické, Trojanova 13, 120 00 Praha 2, Česká Republika*

[2]*Katedra materiálů, Fakulta jaderná a fyzikálně inženýrská, České vysoké učení technické, Trojanova 13, 120 00 Praha 2, Česká Republika*

[3]*Department of Applied Physics, Zernike Institute for Advanced Materials, Faculty of Science and Engineering, University of Groningen, Nijenborgh 4, 9747 AG, Groningen, The Netherlands*

karel.trojan@fjfi.cvut.cz

Cílem tohoto příspěvku je popsat reálnou strukturu laserem navařené nástrojové ocele AISI H13. Byl vytvořen návar z pěti vrstev, na kterém byla následně charakterizována mikrostruktura a fázové složení rentgenovou difrakcí. V rámci tlouš ky navařeného kovu byla nalezena oblast s výrazně nižší tvrdostí a odlišnou mikrostrukturou, což by mohlo negativně ovlivnit vlastnosti nově vytvořeného objemu.

Nástrojová ocel AISI H13 pro práci za tepla je jedním z běžných materiálů používaných v průmyslu pro výrobu forem, zápustek nebo ozubených kol. Formy během své životnosti trpí silným poškozením v důsledku termodynamického namáhání [1]. Proto byly vyvinuty různé způsoby jejich oprav, které jsou levnější než výroba nových forem. Velkou výhodou laserového navařování je vysoká produktivita s minimálním vlivem díky nízkému vnesenému teplu do základního materiálu. Vnesené teplo způsobuje deformace nebo zhoršení vlastností materiálu v důsledku popuštění. Laserové navařování proto umožňuje opravy forem bez dalšího tepelného zpracování [2]. Při navařování více vrstev jsou však předchozí vrstvy tepelně ovlivněny, což může významně změnit jejich mikrostrukturu, reálnou strukturu a tvrdost. Z tohoto důvodu ovlivňuje výslednou tvrdost návaru nejen rychlost ochlazování, ale také teplota dosažená během depozice dalších vrstev [3]. Proto je důležité sledovat a porozumět mikrostrukturálním změnám nově vytvořeného materiálu. Tyto znalosti lze použít k návrhu postupu pro depozici větších objemů.

Obrázek 1. Výbrus návaru s výrazněnou mikrostrukturou.

Laserové navařování bylo prováděno pomocí vláknového laseru IPG 3kW Yt:YAG. Hustota laserového výkonu 90 J/mm^2 byla použita k vytvoření návaru z pěti vrstev, viz obrázek 1. Každá vrstva byla vytvořena ze šesti, nebo sedmi překrývajících se housenek na substrátu z nástrojové oceli AISI H11. Byl použit prášek s průměrným průměrem částic 94 ± 24 m.

Za účelem stanovení fázového složení vrstev byly získány difrakční záznamy na přístroji X'Pert PRO MPD v klasické Braggově–Brentanově konfiguraci s kobaltovým zářením a křížovými clonami 1 × 0,25 mm^2. Difrakční záznamy byly zpracovány programem X'Pert HighScore Plus a jednotlivé fáze byly identifikovány pomocí databáze PDF-2. Kvantitativní analýza byla provedena pomocí Rietveldovy analýzy v softwaru MStruct. Efektivní hloubka vnikání odpovídá tlouš ce povrchové vrstvy, která poskytuje přibližně 63% difraktované intenzity. V případě použité vlnové délky je hloubka vnikání asi 5 m.

Podle výsledků rentgenové fázové analýzy, viz obrázek 2, je podíl austenitu nejvyšší v první navařené vrstvě, přibližně 11 hm. %. Naopak nejnižší podíl, méně než 2 hm. %, je v tmavé oblasti, viz obrázek 1, která zároveň

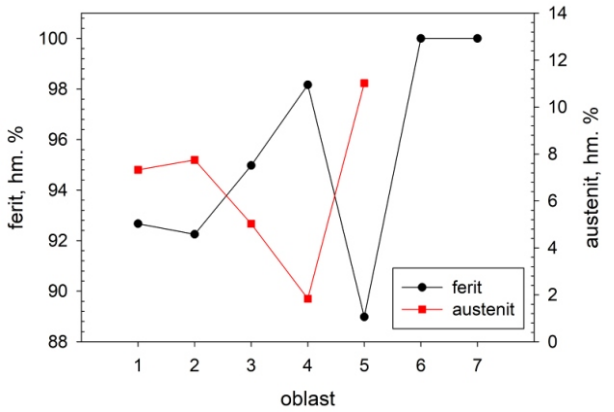

Obrázek 2. Fázové složení jednotlivých navařených vrstev, kde oblast 1 je poslední navařená, 6 TOO a 7 substrát.

vykazuje nižší tvrdost o ca 200 HV_{IT}. Pomocí rentgenové fázové analýzy bylo možné stanovit pouze ferit v tepelně ovlivněné oblasti (TOO) a substrátu. Je vhodné poznamenat, že vzhledem k nízkému obsahu uhlíku v oceli nemůže rentgenová fázová analýza rozlišit mezi feritem, martenzitem a bainitem kvůli nízkému podílu mřížkových parametrů a/c. Karbidy v substrátu nebyly rentgenovou difrakcí pozorovány, pravděpodobně jsou velmi jemné.

Laserové navařování nástrojové oceli H13 vykazuje velký aplikační potenciál. Ukázalo se, že mikrostruktura, fázové složení a tvrdost návaru z více vrstev se v rámci hloubky významně liší. Jedná se o velmi důležité zjištění, protože oblast s nižší tvrdostí by mohla způsobit výrazně nižší životnost na povrchu opravené formy. Výzkumné téma a především formování oblasti s nižší tvrdostí však dosud nebylo přesně popsáno a pochopeno, takže bude zapotřebí dalšího výzkumu.

1. R. G. Telasang, et al. Microstructure and Mechanical Properties of Laser Clad and Post-cladding Tempered AISI H13 Tool Steel. *Metall. Mater. Trans. A.* **46A**: 2309–2321, 2015.
2. M. Vedani, et al. Problems in laser repair-welding a surface-treated tool steel, *Surf. Coat. Tech.* **201**: 4518–4525, 2007.
3. G. Roberts, et al. Tool Steels. *Materials Park: A S M International*, 1998.

Tato práce byla podpořena grantem Studentské grantové soutěže ČVUT č. SGS19/190/OHK4/3T/14 a projektem CZ.02.1.01/0.0/0.0/16_019/0000778 "Center for advanced applied science" v rámci Operačního programu Výzkum, vývoj a vzdělání, který je kontrolován Ministerstvem školství, mládeže a tělovýchovy České Republiky.

SL5

STRUCTURE OF METAL-PLASMA POLYMER Ag/HMDSO NANOPARTICLES AND ITS THERMAL DEVELOPMENT STUDIED BY X-RAY SCATTERING METHODS

Tereza Košutová[1], Lukáš Horák[1], Artem Shelemin[2], Mykhailo Vaidulych[2], Jan Hanuš[2], Hynek Biederman[2], Ondřej Kylián[2], Pavel Solař[2], Miroslav Cieslar[3], Andrei Choukourov[2], Milan Dopita[1]

[1]Department of Condensed Matter Physics, Faculty of Mathematics and Physics, Charles University, Ke Karlovu 5, 121 16 Prague 2, Czech Republic

[2]Department of Macromolecular Physics, Faculty of Mathematics and Physics, Charles University, V Holešovičkách 2, 180 00 Prague 8, Czech Republic

[3]Department of Physics of Materials, Faculty of Mathematics and Physics, Charles University, Ke Karlovu 5, 121 16 Prague 2, Czech Republic

KosutovaT@gmail.com

Nowadays, nanomaterials are certainly a very hot topic in society. The efforts to prepare heterogeneous nanoparticles, i. e. nanoparticles composed of parts from different materials, are driven by their interesting characteristics coming from the combination and synergy of individual materials properties.

This study follows up heterogeneous nanoparticles composed of a silver core and polymeric shell. These so-called core@shell nanoparticles were prepared by a combination of magnetron-based gas aggregation cluster source (GAS) and simultaneous plasma enhanced chemical vapour deposition of hexamethyldisiloxane (HMDSO). A series of Ag nanoparticles prepared at various HMDSO pressure was prepared.

Studied samples differ in the size of the silver core and also in the thickness of the polymeric shell. These properties can be tuned by the amount of HMDSO supplied to the deposition chamber. During the process without HMDSO nanoparticles of size around 40 nm are created on the other hand with 9 % of HMDSO supplied near to the target surface, the diameter of nanoparticles decreases to 5 nm. Size of coherently diffracting domains does not depend on the amount of added HMDSO and stays around 5 nm. Microstrain and density of stacking faults increases with the concentration of HMDSO in the system, the details were published in [1].

Thermal properties of heterogeneous metal-polymer nanoparticles were investigated by methods of small angle x-ray scattering, x-ray diffraction, ultraviolet-visible spectroscopy and electron microscopy. The changes in size distribution, shape, and microstructure of nanoparticles with increasing temperature up to 450 °C were observed and determined.

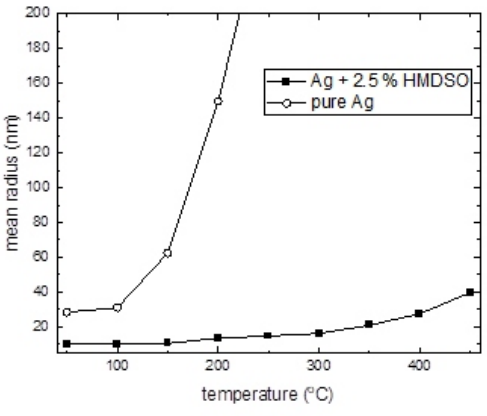

Figure 1. Temperature dependence of nanoparticles silver core diameter for pure silver nanoparticles and nanoparticles prepared with the lowest amount of HMDSO in the aggregation chamber.

XRD patterns of selected samples before and after heating to 450 °C were analysed. With increasing temperature, the ordering of atoms is observed, the decrease in density of stacking faults and relaxation of lattice parameters. Thermal evolution of size for pure silver nanoparticles and the silver cores of nanoparticles prepared with the lowest amount of HMDSO added to the aggregation chamber is depicted in figure 1. The comparison with pure silver nanoparticles shows that the polymeric shell around nanoparticles prevents nanoparticles fusion. The growth of heterogeneous nanoparticles takes place above 350 °C, coalescence temperature for pure silver nanoparticles is below 100 °C.

1. T. Košutová et al., "Synthesis and microstructure investigation of heterogeneous metal-plasma polymer Ag/HMDSO nanoparticles," Surf. Interface Anal., no. 2019, pp. 1-4, 2020, doi: 10.1002/sia.6779.

The authors acknowledge the financial support from the project NanoCent—Nanomaterials Centre for Advanced Applications, Project No. CZ.02.1.01/0.0/0.0/15_003/0000485, financed by ERDF.

Session II

SL6

APPLICATION OF PAIRED REFINEMENT IN FRAGMENT-SCREENING PROJECT

M. Malý[1,2], K. Diederichs[3], J. Dohnálek[2], P. Kolenko[1,2]

[1]Czech Technical University in Prague, Faculty of Nuclear Sciences and Physical Engineering, Břehová 7, 115 19 Prague, Czech Republic

[2]Institute of Biotechnology of the Czech Academy of Sciences, Biocev, Průmyslová 595, 252 50 Vestec, Czech Republic

[3]University of Konstanz, Box M647, 78457 Konstanz, Germany

martin.maly@fjfi.cvut.cz

The paired refinement protocol [1] is considered as the optimal approach for the determination of high-resolution cutoff in macromolecular crystallography. Unlike the conservative criteria based only on the indicators of diffraction data quality, it enables a direct linking of the quality of data and structure model. Generally, the proper estimation of the resolution limit reduces the noise level in calculated electron density maps which subsequently leads to finer molecular structures. Especially, this has an impact on regions difficult to interpret.

During our recent work on *PAIREF* – automation of the protocol [2] – we analysed the data set from endothiapepsin from *Cryphonectria parasitica* in complex with fragment B53 [3], PDB entry 4Y4G. However, the mentioned ligand (molecule of fragment B53) is occupied only partially. Despite the importance of determination of exact molecule position, the signal is rather weak in this region.

Although the structure was previously solved at 1.44Å resolution, we reprocessed the data in *XDS* [4] and performed paired refinement in *PAIREF* using *REFMAC*5 [5] up to 1.05 Å. Obtained results showed the data contain useful signal up to 1.20 Å. Moreover, the clear evidence of improvement of electron density quality in ligand region was observed while the optimal high-resolution cutoff was applied (Figure 1).

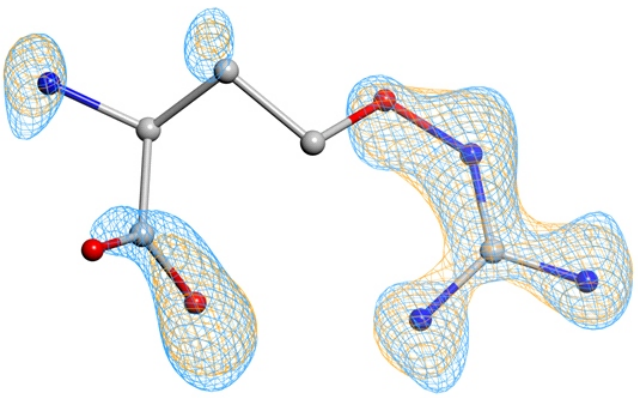

Figure 1. Comparison of electron-density omit maps of the partially occupied fragment B53 after refinement at 1.44 Å (orange) and 1.20 Å (blue) – contoured at 0.56 e·Å^{-3} level. Atomic coordinates originate from PDB entry 4Y4G [3]. The figure was created in *CCP4mg* [6].

1. P. A. Karplus & K. Diederichs, *Science*, **336**, (2012), pp. 1030–1033.
2. M. Malý, K. Diederichs, J. Dohnálek, P. Kolenko, *IUCrJ*, **7**, (2020), pp. 681–692.
3. F. Huschmann, J. Linnik, K. Röwer, M. Ühlein, X. Wang, A. Metz, J. Schiebel, A. Heine, G. Klebe, M. Weiss, U. Mueller, *Acta Cryst. D*, **72**, (2016), pp. 346–355.
4. W. Kabsch, *Acta Cryst. D*, **66**, (2010), 125.
5. G. N. Murshudov, A. A. Vagin, E. J. Dodson, *Acta Cryst. D*, **53**, (1997), pp. 240–255.
6. S. McNicholas, E. Potterton, K. S. Wilson, M. E. M. Noble, *Acta Cryst. D*, **67**, (2011), pp. 386–394.

This publication was supported by the MEYS CR (projects CAAS – CZ.02.1.01/0.0/0.0/16_019/0000778 and BIOCEV – CZ.1.05/1.1.00/02.0109) from the ERDF fund and by the GA CTU in Prague (SGS19/189/OHK4/3T/14).

SL7

STRUCTURAL STUDIES OF PURINE NUCLEOSIDE PHOSPHORYLASE INHIBITORS

S. Djukic[1], J. Skácel[1], J. Brynda[1,2], P. Pachl[1], T. Vučková[1], M. Fábry[2], J. Snášel[1], M. Rumlová[3], T. Bílek[1,3], J. Voldřich[1,3], H. Mertlíková-Kaiserová[1], Z. Janeba[1], P. Řezáčová[1,2]

[1]Institute of Organic Chemistry and Biochemistry, AS CR, Prague 6, Czech Republic
[2]Institute of Molecular Genetics, AS CR, Prague 4, Czech Republic
[3]University of Chemical Technology, Prague 6, Czech Republic
Stefan.dukic@uochb.cas.cz

Nucleic acid synthesis and degradation are ongoing metabolic processes in most cells. The degradative processes lead to the release of free purines and the salvage pathway exists to recover them efficiently in a useful form. Purine nucleoside phosphorylase (PNP) represents one of the key enzymes of the purine salvage pathway, which is considerably more energy-efficient than *de novo* pathway. It hydrolyses ribose from inosine and guanosine in the presence of an inorganic phosphate, producing hypoxanthine and guanin, which can then be recycled trough the salvage pathway or be further degraded to uric acid.

Human PNP activity is increased in T-cell leukemia, breast and colon cancer and during autoimmune diseases. It is also found to cleave antiviral drugs and to play a role in immune response, which leads to transplant-organ rejection. PNP is conserved in most organisms, and for lot of parasitic organisms like *Mycobacterium tuberculosis* (tuberculosis causing agent) and *Plasmodium falciparum* (malaria causing agent) it more favorable, if not the only way to obtain purines. Thus, human PNP, as well as parasitic PNPs, have been established as prospective targets for drug design with several PNP inhibitors recently entered human clinical trials. Due to structural similarities between PNPs in different organisms, it is a serious challenge to design selective inhibitors making structural studies of PNPs an important task.

Human PNP is a functional homotrimer. Parasitic PNPs are either trimers (*Mtb*PNP) or hexamers (*Pf*PNP). Each subunit has an active site which is formed mostly by the parent subunit with one or few participating residues belonging to neighboring subunit.

We are using X-ray crystallography in structure-based drug design of novel acyclic nucleotide analogues. Our goal is to design inhibitors with high affinity towards hPNP as well as *Mtb*PNP and *Pf*PNP.

Enzymes were prepared by heterologous expression in *E. coli* and purified in high yields and purity necessary for crystallographic studies. Crystallization conditions for all three enzymes were identified through wide screening and optimization. Selected inhibitors with affinity in nanomolar range were successfully co-crystallized with hPNP and *Mtb*PNP, diffraction data have been collected on BL14.1 at the BESSY II electron storage ring operated by the Helmholtz-Zentrum Berlin and crystal structures were determined at high resolution (Figure 1).

The knowledge of binding properties of these inhibitors will provide us crucial information which will be used to further optimize affinity and selectivity of new generation of PNP inhibitors.

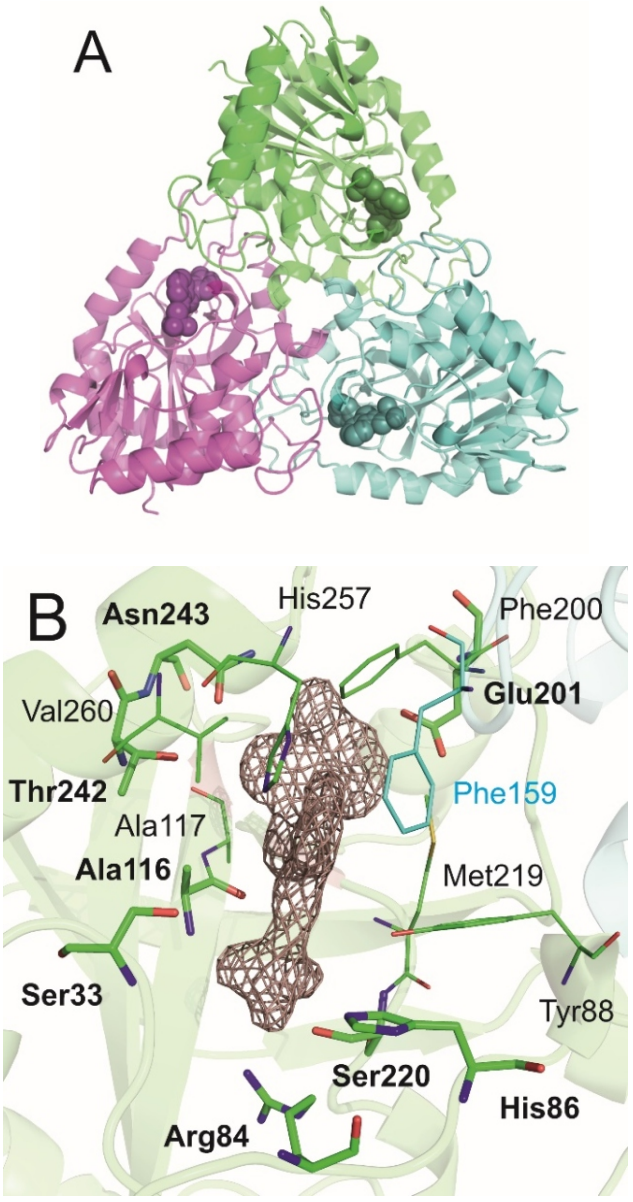

Figure 1. Crystal structure of human PNP in complex with one of the inhibitors. **A**-Overall structure of the trimer, with each subunit being colored differently. Inhibitor atoms are represented as spheres in the same color as parent subunit. **B-** Active site of the same hPNP:inhibitor structure. Hydrogen-bond forming residues are represented with sticks and marked in bold, while other binding-interface-forming residues are represented as lines. Neighboring subunit is represented with cyan color. *2Fo-Fc* electron density map, contoured at 1.3 is shown for ligand bound to the enzyme active site.

SL8

EXPERIMENTAL AND COMPUTATIONAL INVESTIGATIONS OF THE HALOALKANE DEHALOGENASES AND THEIR INTERACTIONS WITH IONIC LIQUIDS

A. Shaposhnikova[1], T. Prudnikova[1], B. Minofar[2], I. Kuta Smatanova[1]

[1]Faculty of Science, University of South Bohemia in Ceske Budejovice, Czech Republic
[2]Institute of Microbiology of the Czech Academy of Sciences, Nove Hrady, Czech Republic

Haloalkane dehalogenases (HLDs) are microbial enzymes that catalyze the cleavage of a carbon-halogen bond by a hydrolytic mechanism. The reaction products are halide ion, hydronium ion (proton) and an alcohol molecule. These enzymes can be useful for the biodegradation of many important environmental pollutants such as 1,2-dichloroethane, 1,2,3,4,5,6-hexachlorocyclohexane, and 1-chlorobutane [1].

The haloalkane dehalogenase DhaA from *Rhodococcus rhodochrous* is a monomeric enzyme with molecular weight of 34 kDa and it is a representative of the large superfamily of hydrolases [1]. Mutant variant DhaA80 with enhanced structural and kinetic stability in the presence of dimethyl sulfoxide and the elevated temperature was constructed by directed evolution and site-directed mutagenesis. The crystallization experiment was performed using the sitting-drop vapor-diffusion method at a temperature of 4°C. Crystals of DhaA80 grown from the precipitant containing 20% PEG 3350, 0.2M sodium fluoride and ionic liquids (IL) from *Hampton Research Ionic Liquid Screen - HR2-214*. Crystals diffracted to the resolution of 1.8 Å. The known structure of HLD from *Rhodococcus* sp. (*www.rcsb.org*) was used as a template for molecular replacement. The structures of DhaA80 including IL solutions containing 1) 50% w/v 2-Hydroxy-ethylammonium formate, 2) 50% w/v 1-Butyl-3-methylimidazolium dicyanamide and 3) 50% w/v 1-Butyl-3-methylimidazolium methyl sulfate were solved after several refinements and validations. For further research and understanding, the interaction of ILs ions molecular dynamics (MD) simulations have been used. MD simulations of systems containing DhaA80 with 50% w/v 1-Butyl-3-methylimidazolium methyl sulfate and 50% w/v 2-Hydroxy-ethylammonium formate have been performed. The analysis of MD data by using root mean square deviation (RMSD) and root mean square fluctuations (RMSF) confirmed that ILs affect the structure and stability of enzyme.

1. T. Prudnikova, R. Chaloupkova, Y. Sato, Y. Nagata, I. Kuta Smatanova et al. Development of a Crystallization Protocol for the DbeA1 Variant of Novel Haloalkane Dehalogenase from Bradyrhizobium elkani USDA94. *Crystal Growth & Design*, **11(2)**, 516–519 (2011).
2. P. Vanacek, E. Sebestova, P. Babkova, S. Bidmanova, L. Daniel, P. Dvorak, V. Stepanova, J. Damborsky et al. Exploration of Enzyme Diversity by Integrating Bioinformatics with Expression Analysis and Biochemical Characterization. *ACS Catalysis*, **8(3)**, 2402–2412 (2018).

SL9

PRODUCTION OF TBEV NS5 PROTEIN FOR STRUCTURAL STUDIES

Petra Havlíčková[1], Zdeno Gardian[1, 2], Paulina Duhita Anindita[1], Ivana Kutá Smatanová[1], Roman Tůma[1] and Zdeněk Franta[1]

[1]Institute of Chemistry, Faculty of Science, University of South Bohemia, Branišovská 1760, České Budějovice, Czech Republic
[2]Institute of Parasitology, Biology Center of the Czech Academy of Sciences, České Budějovice, Czech Republic
zfranta@prf.jcu.cz

Tick-borne encephalitis virus (TBEV) is a major human pathogen, transmitted by ticks from family *Ixodidae* [1, 2]. TBEV is an enveloped virus with a ~ 11 kb positive-sense single-strand RNA genome that encodes a single 375 kDa polyprotein. During the infection in the host cells, the polyprotein is cleaved by cellular and viral enzymes into three structural (capsid (C), pre-membrane (prM) and envelope (E)) and seven non-structural (NS1, NS2A, NS2B, NS3, NS4A, NS4B and NS5) proteins [3]. While structural proteins are involved in the architecture of new virions [4], non-structural proteins are responsible for the virus replication, forming replication complex [5].

Non-structural protein NS5 is a large bi-functional protein comprising of two domains connected by highly flexible 10aa linker, which is important for RdRp activity as well as for the overall shape of the protein. N-terminal methyltransferase (MTase) domain is involved in the capping process. C-terminal part of the protein displays RNA-dependent RNA polymerase (RdRp) activity, crucial for virus replication [6].

This project focuses on structural studies of TBEV NS5 protein. Various constructs of TBEV NS5 protein were designed: a – full length NS5 full length including both domains, b – RdRp domain + 10aa linker, c – RdRp domain + 8aa linker, d – RdRp domain without linker, e – MTase do-

main. Expression and purification of individual constructs was optimized and pure samples were used for initial crystallization screening applying various commercially available crystallization screens (Molecular Dimensions, Hampton Research) as well as for cryo-EM analysis.

So far, we have obtained preliminary cryo-EM data for RdRp domain, showing typical flavivirus RdRp structure at 11 Å, that will be further refined. Needle shaped protein crystals of RdRp domain grew in several crystallization conditions. Their protein origin was verified by UVEX imaging system and these conditions will be further optimized by microseeding technique in order to grow more suitable protein crystals for X-ray diffraction analysis.

1. Bogovic, P. & Strle, F. (2015). *Word J. Clin. Cases.* **3**, 430.
2. Taba, P., Schmutzhard, E., Forsberg, P., Lutsar, I., Ljostad, U., Mygland, A., Levchenko, I., Strle, F. & Steiner, I.(2017). *Eur. J. Neurol.* 24, 1214-1261.
3. Lindenbach, B. D., Murray, C. L., Thiel, H. J. & Rice, C. M. (2013). In *Fields Virology.* Lippincott Williams & Wilkins, PA, USA.
4. Fuzik, T., Formanova, P., Ruzek, D., Yoshii, K., Niedrig, M. & Plevka, P. (2018). *Nat. Commun.* **9**, 436.
5. Mackenzie, J. (2005). *Traffic.* **6**, 967-977.
6. Bollati, M. *et al.* (2009). *Antiviral Res.* **87**, 125-148.

This research is supported by ERDF No. CZ.02.1.01/ 0.0/0.0/15_003/000041.

SL10

STRUCTURE COMPARISON OF SALIVARY SERPINS FROM *IXODES RICINUS*

Barbora Kaščáková[1], Tatyana Prudnikova [1], Jindřich Chmelař[2] and Ivana Kutá Smatanová [1]

[1]Institute of Chemistry, Faculty of Science, University of South Bohemia, Branišovská 1760, České Budějovice, Czech Republic

[2]Department of Medical Biology, Faculty of Science, University of South Bohemia, Branišovská 1760, České Budějovice, Czech Republic

barbora.karaffova@gmail.com

Serine protease inhibitors-serpins is a group of ancient proteins widely distributed in nature [1]. Serpins function as serine protease inhibitors but during the evolution, some serpins lost their inhibitory function and serve as molecular chaperones (Heat shock serpin 47), tumor suppressors (Maspin), hormone transporters (Cortisol-binding globulin) or as storage proteins (Ovalbumin) [2]. Inhibitory serpins vary in functions according to their specificity and their importance is stressed by serpinopathies, diseases caused by serpin dysfunction or deficiency. Many of today well-known diseases, such as emphysema, cirrhosis, angioedema, hypertension and familial dementia, are associated at least partially by serpin dysfunction [3]. This makes serpins interesting candidates for drug development and knowledge of detailed serpin structure is necessary for it.

1. Silverman GA, Bird PI, Carrell RW, et al. The serpins are an expanding superfamily of structurally similar but functionally diverse proteins. Evolution, mechanism of inhibition, novel functions, and a revised nomenclature. J Biol Chem. 2001;276(36):33293-33296. doi:10.1074/jbc.R100016200.
2. Law RH, Zhang Q, McGowan S, et al. An overview of the serpin superfamily. Genome Biol. 2006;7(5):216. doi:10.1186/gb-2006-7-5-216.
3. Sanrattana W, Maas C, de Maat S. SERPINs-From Trap to Treatment. Front Med (Lausanne). 2019;6:25. Published 2019 Feb 12. doi:10.3389/fmed.2019.00025.

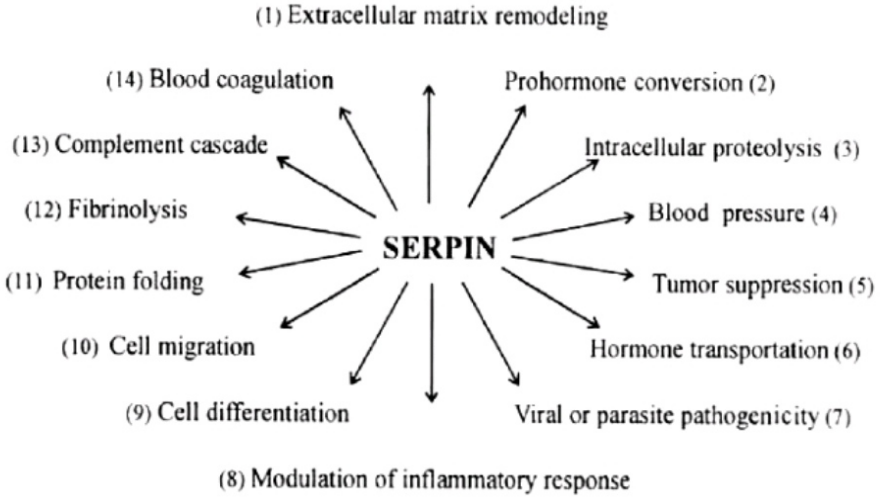

Figure 1 Multiple regulatory functions of serpins (From Koiou *et al*., 2011).

SL11

X-ray diffraction analysis of flavin-dependent oxidase from thermophil Chaetomium thermophilum

RENTGENOVÁ DIFRAKČNÍ ANALÝZA FLAVIN-DEPENDENTNÍ OXIDÁZY Z TERMOFILNÍ HOUBY *CHAETOMIUM THERMOPHILUM*

A. Kravic[1], L. Švecová[1, 2], P. Kolenko[1, 2], L. H. Østergaard[3], J. Dohnálek[2]

[1]Fakulta Jaderná a Fyzikálně Inženýrská, České vysoké učení technické v Praze, Břehová 7, 115 19 Praha 1, Česká republika

[2]Biotechnologický ústav Akademie Věd České republiky, Biocev, Průmyslová 595, 252 50, Vestec, Czech Republic

[3]Novozymes A/S, Biologiens Vej 2, 2800 Kgs. Lyngby, Dánsko

kraviale@fjfi.cvut.cz

Flavin-dependentní oxidoreduktáza z termofilní houby *Chaetomium thermophilum* (CtFDO) je monomerní termostabilní glykoprotein. U této oxidoreduktázy CtFDO se očekává katalýza dvouelektronové oxidace primárních a sekundárních alkoholů doprovázena dvouelektronovou redukcí molekulárního kyslíku na peroxid vodíku. Pro svou aktivitu vyžaduje CtFDO oxidovaný (planární) stav kofaktoru FAD [1]. Ve všech strukturách tohoto proteinu se vyskytuje FAD v redukovaném (neplanárním) stavu. Oxidovaný stav FAD nebyl doposud ve strukturách CtFDO pozorován [2].

Pomocí vysoce intenzivního domácího zdroje rentgenového záření (D8 Venture) jsme se pokusili naměřit enzym CtFDO v oxidovaném stavu. Dále jsme se pokusili pozorovat postupnou redukci FAD v zavilosti na absorbované dávce záření. Naměřená difrakční data byla zpracována po segmentech, které vykazovaly dostatečnou kompletnost a rozlišení k pozorování strukturní změny FAD. Tato data jsme zpracovali programů XDS [3] a AIMLESS [4], struktura byla upřesněna pomocí programu REFMAC5 [5].

Již první segment poukazuje na redukovaný stav FAD. Na dalších segmentech difrakčních dat byla pozorována fluktuace elektronové hustoty v místě FAD. Nově navržené experimenty zohledňují tyto výsledky a povedou k pozorování oxidovaného stavu FAD ve struktuře enzymu CtFDO.

1. Li, A.-N.; Li, D.-C.: *J. Appl. Microbiol.* 2009, 106, p. 369-380.
2. Švecová L.; Skálová T.; Kovaľ T.; Řstergaard L. H.; Kolenko P.; Dušková J.; Dohnálek J.: *So, what does the enzyme do? Structural data-based identification of substrate specificity*, 2018, Qeudlinburg, Germany (presentation).
3. Kabsch W.: *XDS*. Acta Cryst., 2010, D66, s. 125–132.
4. Evans P. R.; Murshudov G. N.: *How good are my data and what is the resolution?* Acta Cryst., 2013, D69, s. 1204–1214.
5. Murshudov G. N. et al.: *REFMAC5 for the refinement of macromolecular crystal structures*. Acta Cryst., 2011, D67, s. 355-367.

Tato práce byla podpořena Grantovou agenturou ČVUT v Praze (SGS19/189/OHK4/3T/14) a projekty MŠMT (CAV - CZ.02.1.01/0.0/0.0/16_019/0000778).

SL12

ATOMIC RESOLUTION STRUCTURES OF S1 NUCLEASE COMPLEXES REVEAL DETAILS OF RNA INTERACTION WITH ENZYME IN SPITE OF UNUSUAL CRYSTAL DEFECT

K. Adámková[1,2], T. Kovaľ[1], L. H. Østergaard[3], J. Dohnálek[1]

[1]Institute of Biotechnology of the Czech Academy of Sciences, v.v.i., Biocev, Průmyslová 595, 252 50 Vestec, Czech Republic

[2]University of Chemistry and Technology Prague, Department of Biochemistry and Microbiology, Technická 5, 166 28 Prague 6, Czech Republic

[3]Novozymes A/S, Biologiens Vej 2, 2800 Kgs. Lyngby, Denmark

adamkovak@ibt.cas.cz

S1 nuclease from *Aspergillus oryzae* is a zinc-dependent phosphoesterase from the S1-P1 family of nucleases cleaving nucleic acids to nucleotides. Enzymes of the family can be found in many species having various biological functions with potential utilization in biotechnology and biochemistry. These enzymes have the phospholipase C/P1 nuclease fold and almost the same active site features, including the trinuclear zinc cluster, yet their substrate specificity differs from the strictly single-strand-specific to the non-specific nucleases able to cleave RNA, ssDNA, as well as dsDNA. Even though, the cleavage mechanism of the S1-P1 family enzymes was already described and there

are several structures of complexes with products/ligands bound in the active site, there are still questions related to their substrate specificity and preferences [1, 2].

To further increase our understanding of the mechanisms behind the substrate specificity, we performed co-crystallization of S1 nuclease with various products of DNA and RNA cleavage. We obtained two novel structures of S1 nuclease in complex with RNA cleavage products in the active site. A complex with cytidine-5'-monophosphate at 1.05Å resolution and a complex with uridine at 1.10Å resolution. The atomic resolution of both structures enables observation of fine details of ligand binding in the active site of the S1 nuclease and also a detailed comparison with already known complexes.

Both structures feature several unexpected strong peaks at 10 level of difference electron density (mF_O-DF_C), incompatible with standard molecular geometry constraints and not interpretable within the coordinates of the enzyme and its ligands. A closer analysis suggests that they correspond to zinc ions of translated protein molecules along the *c* axis of the unit cell. The translated molecules are present at low partial occupancy in two different positions and can be most likely interpreted as an intriguing case of order-disorder in protein crystal.

1. Kovaľ T, Dohnálek J, *Biotechnology Advances*, 2018, 36(3): 603-612

2. Kovaľ T. *et al*., *PLoS ONE*, 2016, 11(12): e0168832.

This work was supported by the Academy of Sciences of the Czech Republic (RVO: 86652036) and European Regional Development Fund (Project CIISB4HEALTH, No. CZ.02.1.01/0.0/0.0/16_013/0001776 and ELIBIO, No. CZ.02.1.01/0.0/0.0/15_003/0000447).

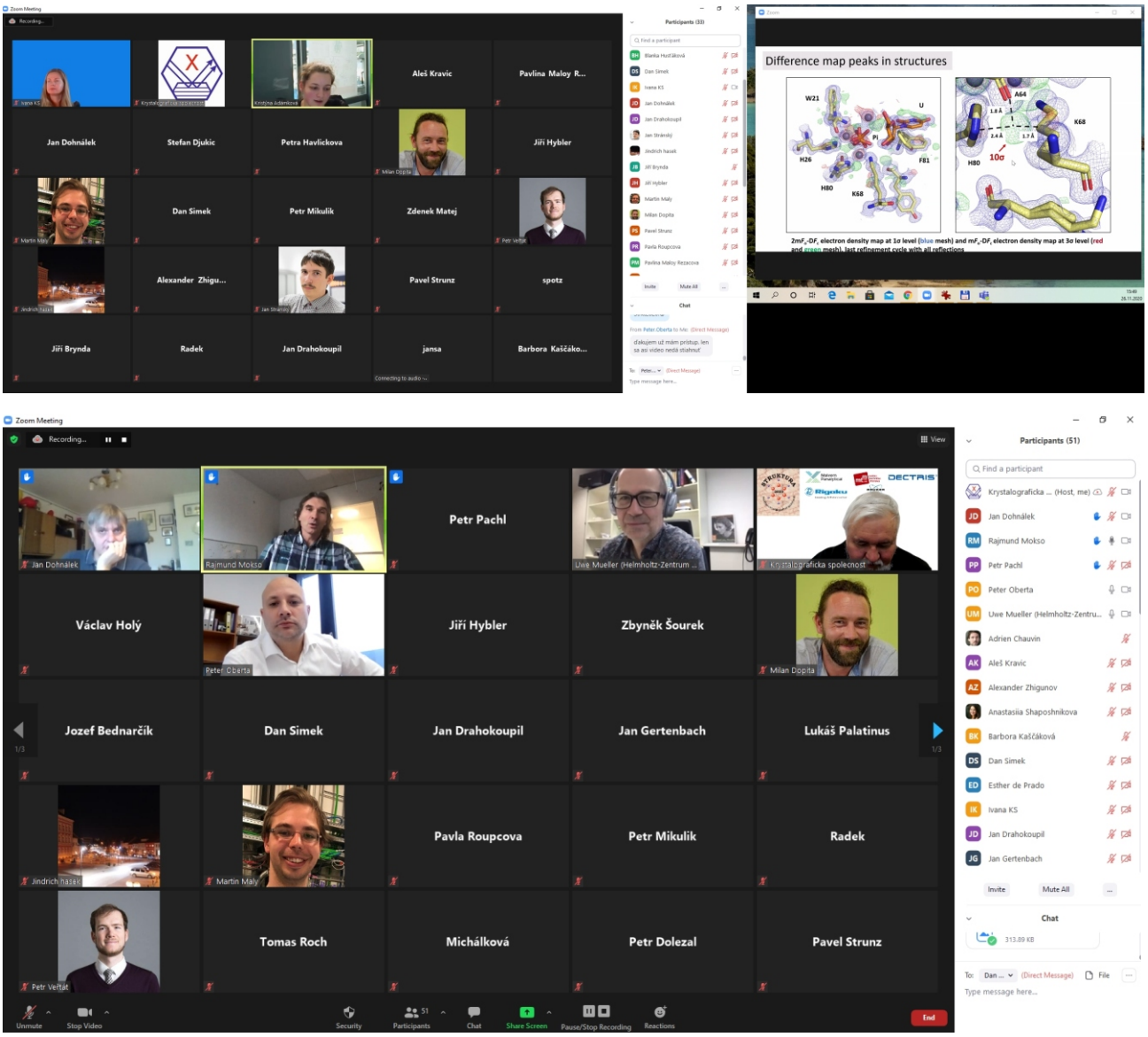

From the conference on screens